Erosion of EUROFER steel by mass-selected deuterium ion bombardment

K. Sugiyama, M. Balden, S. Elgeti, T. Höschen, M. Oberkofler, J. Roth and W. Jacob*

Max-Planck-Institut für Plasmaphysik, Boltzmannstrasse 2, Garching D-85748, Germany

Abstract

The erosion behaviour of EUROFER steel due to mono-energetic deuterium (D) ion bombardment in the energy range of 100 - 1000 eV/D was investigated. At low fluences, the sputtering yield is comparable to that of pure iron (Fe). It then decreases with increasing fluence and tends toward a steady state at larger fluences. The largest experimentally investigated fluences are of the order of several 10^{24} D/m^2. The yield reduction is more pronounced for lower D impinging energies. A simple model is presented within which the evolution of the yield can be described by an exponential decay, using empirical values for the fitting parameters. In this model, the yield reduction is caused by preferential sputtering of Fe and the consequent development of a tungsten- (W-) enriched surface layer. SDTrimSP simulations also confirm the appearance of a W-enriched surface layer. However, the experimentally observed fluence dependence of the sputtering yield could not satisfactorily be reproduced in these simulations. The resulting enrichment layer thicknesses below 1 Å stretch the physics model implemented in SDTrimSP beyond its validity range. Experimentally, surface enrichment of W was qualitatively confirmed in Rutherford backscattering and sputter X-ray photoelectron spectroscopy measurements. However, the measured depth profiles are very likely influenced by the observed surface roughening caused by the D irradiation. Electron microscopy revealed the inhomogeneous W distribution on the un-irradiated sample as well as a grain-dependence of erosion and grain-dependent topography development. The inclusion of surface topography in the description of the erosion could be the key to improve the agreement between model predictions and the experiment.

Keywords: RAFM steel, Erosion, Plasma-material interactions
PACs No.: 52.40Hf, 28.52.Fa, 79.20.Rf, 68.35.bd

* Corresponding author: Wolfgang.Jacob@ipp.mpg.de

1. Introduction

Reduced-activation ferritic martensitic (RAFM) steel, such as EUROFER [1], is planned to be used as structural material in future fusion reactors [2, 3, 4]. For most areas of the first wall, which are subjected to significant fluxes of energetic charge exchange neutral atoms from the plasma, it is foreseen to coat the RAFM steel with tungsten (W) films with thicknesses of the order of 1-2 mm [4, 5]. To avoid the technologically challenging and expensive step of W coating, it would be attractive to use bare steel as a plasma-facing material in recessed wall regions with only negligible impurity ion fluxes and moderate charge-exchange particle fluxes [6].

The erosion rate is one of the main criteria affecting the suitability of a bare steel wall, because it determines the lifetime of plasma-facing components. In recessed areas, the plasma-facing surface is bombarded predominantly by charge-exchange neutrals of hydrogen isotopes. The energy distribution of this particle flux has contributions from a broad range but peaks strongly at low energies [7, 8].

RAFM steel is a compound material consisting of iron (Fe) as the base material, typical mid-Z steel elements (e.g. chromium (Cr), vanadium, manganese) as well as small amounts of high-Z elements such as tungsten (W) and tantalum (Ta) (~0.33 at.% and ~0.04 at.% for EUROFER) [9]. Since the sputtering yield of Fe and the other mid-Z elements is significantly higher than that of the high-Z elements [10], one can expect that during erosion the surface composition will change due to preferential sputtering of low- and mid-Z elements, resulting in an enrichment of high-Z elements. This change of surface composition could be expected to have a direct effect on the erosion behaviour of RAFM steels.

In view of this expectation, exposures of RAFM steels to energetic deuterium (D) plasmas have recently been performed in linear plasma devices [11, 12, 13]. The results obtained in PISCES-A clearly show the anticipated behaviour, namely an increase of the surface W concentration and a reduction of the total erosion yield [12]. The employed linear plasma devices feature high D fluxes so that relatively high fluences can be achieved within reasonable time. However, they in general suffer from intrinsic uncertainties regarding the plasma composition as well as the energy distribution of the impinging species. The energy of the impinging ions depends on the acceleration in the sheath in front of the samples. The acceleration voltage is determined by the plasma potential and a possibly applied bias voltage. Collisions in the sheath cause a broadening of the energy distribution and, possibly, an additional flux of charge-exchange neutrals, which is difficult to determine. Furthermore, the energy distribution (including ions and neutrals) in a specific exposure also depends critically on the applied plasma parameters. The plasma composition is an even more critical issue. In general, the ion flux from a deuterium plasma consists of several molecular ions, usually D^+, D_2^+ and D_3^+ (see for example Refs. [14, 15]). The relative contribution of the various molecular ions depends sensitively on plasma discharge conditions. In addition, the plasma inevitably contains small amounts of impurities, e.g. carbon and oxygen, which either stem from the residual background gas or from the interaction of the plasma with the chamber walls. At low ion energies, particular care must be taken because the sputtering yield can be dominated by such impurities. Finally, if the plasma in front of the target holder is

sufficiently dense, atoms sputtered from the sample or the target holder can be ionized and redeposited onto the substrate. Altogether, the interpretation of data from experiments using plasma exposure is seldom straightforward and can be affected by considerable uncertainties. This motivated us to perform erosion experiments under well-defined conditions to obtain a consistent set of reliable data for sputtering of EUROFER by energetic D ions.

In this study, the erosion of EUROFER steel is investigated using the high current ion source setup HSQ of IPP [10, 16], which is able to deliver a mono-energetic mass-selected D ion beam. Sputtering yields are assessed as functions of fluence at several ion energies. The results are compared to a simple model as well as to SDTrimSP simulations. The surface topography evolution accompanying the erosion is studied by post-irradiation analyses and visualized in SEM images.

2. Experimental procedure

2.1. Sample preparation and deuterium ion irradiation

The samples for this study were cut from a sheet of EUROFER97-2 (heat 993393, originally produced in 2005 for Forschungszentrum Karlsruhe, Germany) with dimensions of 12 mm×15 mm×0.6 mm. The surface to be exposed to the ion beam was mechanically polished to a mirror-like finish. Finally, samples were ultrasonically cleaned in isopropanol to remove residue from polishing.

The samples were then irradiated by D ions in the high current ion source setup (HSQ) [10, 16] at IPP Garching. The HSQ is equipped with a beam deflection magnet, which provides the mass separation of the ion beam at the chosen primary acceleration voltage. As bombarding ion species the D_3^+ molecular ion was chosen, because this is the most abundant ion species extracted from the ion source under our experimental conditions. The bombardment energy at the target is controlled by the primary acceleration voltage and the sample biasing. The molecular D_3^+ ions are considered to be equivalent to three individual D ions impinging at the same velocity as the molecular ions. This assumption is vindicated by the fact that the ion energies are far greater than the molecular binding energies. Effects due to superposition of collision cascades are neglected. Consequently, the exposure to D_3^+ ions is assumed equivalent to the exposure to D^+ ions, whereby the energy per deuteron is 1/3 of the experimentally applied ion energy and the deuteron flux is three times the measured ion flux. In the following, all bombardment energies are given as energy per deuteron (eV/D). The selected D bombardment energies in this study were 100, 200, 500 and 1000 eV/D. The incident angle of the ion beam was normal to the sample surface. The ion flux was determined by measuring the ion current at the sample and dividing by the area of the ion beam footprint. This footprint area was assessed by means of ellipsometry after exposure of an amorphous hydrocarbon layer on a silicon substrate. The sample stage is surrounded by a negatively biased cylindrical cage in order to suppress secondary electron emission due to the ion bombardment. The applied secondary electron suppression ensures an accurate ion current measurement. The deuteron flux is typically of the order of 10^{19} D/m^2/s. The irradiation fluence was varied in the range

from 10^{21} to 10^{24} D/m^2. Accordingly, the exposure times for the highest fluences were approximately 30 hours. The sample was not actively cooled during irradiation. Therefore, the sample was slightly heated by the ion bombardment to temperatures between 310 and 350 K depending on the ion impinging energy. The base pressure in the irradiation chamber was of the order of 10^{-8} mbar. The pressure during irradiation was several 10^{-7} mbar. Under these conditions, no thermal segregation or interdiffusion and negligible surface oxidation are expected.

2.2. Assessment of sputtering yields and post-irradiation analyses

The sputtering yield was evaluated by weight loss measurements. The weight change of each sample due to ion beam exposure was measured ex situ utilizing a microbalance system with a weight resolution of 1 μg and a measurement reproducibility of ± 3 μg. The experimental uncertainty is particularly large for the lowest sputtering yields and at the lowest fluences, where the measured weight loss could be of the order of 10 μg. For most data points, the total weight loss was in the range of several 10 to above 100 μg. The sputtering yield was calculated from the weight loss and the total number of impinging deuterons. For the conversion of the weight loss to the number of sputtered atoms, we assumed that the weight loss is predominantly due to the sputtering of Fe and that contribution of other sputtered elements to the weight change is negligible. The sputtering yields are accordingly given as removed Fe atoms per impinging D. For the trace elements in EUROFER, this is a valid assumption. For Cr, the second largest contribution to EUROFER, we assume that the sputtering yield is very similar to that of Fe (see Ref. [10]) and that the mass difference between Cr (52 amu) and Fe (56 amu) can be neglected. All steel constituents other than W are sputtered together with the Fe atoms with the corresponding atomic ratio. The sputtering threshold for D on pure W lies roughly at 220 eV [10]. It can be shown that due to the presence of Fe and the possibility of sequential collisions between D, Fe and W this threshold is reduced to approximately 100 eV. At impinging D energies of 100 eV it is therefore certainly a good approximation to neglect the contribution of W sputtering to the weight loss. At higher energies, W sputtering can contribute to the weight loss principle. The related systematic error is however expected to be small: The sputtering yield of pure W by D e.g. at 1 keV is more than one order of magnitude lower than that of pure Fe and pure Cr. This approximation to neglect W sputtering is corroborated by SDTrimSP simulations taking into account W enrichment, which show that at 1 keV the sputtered W atoms amount to less than 0.5% of the total sputtered atoms at any fluence. The measurement error was calculated by error propagation from the measurement uncertainty of the weight loss and that of the deuterium fluence. The uncertainty in the weight measurements dominates the error bars at low fluences, while at higher fluences the uncertainty in the fluence determination is dominant. The fluence uncertainty itself is dominated by the determination of the beam footprint area, which does not have perfectly sharp edges. The footprint area and shape are practically the same for implantations with a given impinging energy, but they vary with the D impinging energy (the area size varies from about 0.5 to about 0.9 cm^2). An uncertainty of 20% due to this systematic error in the footprint area determination

is assumed as an upper estimate. For each investigated D bombardment energy, several individual samples (typically three or four) were used in order to check the reproducibility as well as to prepare a set of samples for the post-irradiation surface analyses described further below.

Elemental depth profiles were measured by Rutherford backscattering spectroscopy (RBS) and X-ray photoelectron spectroscopy (XPS). RBS was performed in the Cornell geometry using 1.0 MeV $^4He^+$ ions and a typical dose of 10 μC. The sample was tilted to achieve an incident angle of 75° with respect to the surface normal in order to enhance the depth resolution at the surface. The backscattered ^4He was analysed by a solid-state detector located at a scattering angle of 165°. According to RESOLNRA [17] the depth resolution in Fe under these experimental conditions is approximately 3×10^{16} at./cm^2, i.e. about 3.5 nm. However, as can be seen in the next section, this resolution was not achieved due to the influence of surface roughness.

XPS spectra were acquired on some selected samples using a PHI 5600 ESCA system equipped with an Al K_α X-ray source. Depth profiling was performed by sputter-erosion using a beam of 10 keV Ar^+ ions at an incident angle of 20°, and periodically recording the photoelectron spectra.

The surface morphology before and after D ion irradiation was examined by scanning electron microscopy (SEM).

3. Results and discussion

3.1. Fluence and energy dependence of the sputtering yield

3.1.1. Experimental results

Figure 1 shows the sputtering yields as a function of D fluence for various D bombardment energies. Weight measurements were carried out before irradiation and after chosen fluence intervals up to the final fluence. The sputtering yield was then determined from the weight loss in each fluence interval and the corresponding incremental fluence. Thus, the resulting sputtering yield values are 'discrete' differential sputtering yields, i.e. averaged over fluence intervals. These intervals are small enough to make a comparison to differential sputtering yields (as they result e.g. from SDTrimSP simulations) reasonable.

In cases of low fluence the weight change is relatively small (around 10 μg, which is comparable to the measurement uncertainty), leading to large scatter of the data and large error bars. A possible influence of any surface oxide would also more strongly affect the results in the lower fluence range: On an oxidized surface, the apparent sputtering yield of Fe (and other constituents) could be significantly reduced. A study of Fe sputtering by hydrogen ion irradiation using laser-excited fluorescence spectroscopy [18] revealed that the sputtering yield of Fe at the onset of irradiation was much lower than expected, whereas it increased after removal of about 20 monolayers from the surface. If the thickness of the oxide layer on the EUROFER steel samples used in this study is assumed similar to that in Ref. [18], its influence on the sputtering yields would not be measurable: Within the error bars the yield at

low fluences corresponds to that of pure Fe. An influence of a surface oxide layer on these sputtering yield measurements is therefore neglected.

At higher fluences, the weight change within one fluence interval is larger (in the range from several tens to above 100 μg), resulting in a smaller scatter of the data points and smaller error bars. As mentioned, at low fluences the yield is roughly similar to that of Fe, whereas it starts decreasing at fluences of 10^{23} D/m^2. The yield reduction is more pronounced for lower D bombardment energies. In the high fluence range of 3 - 4×10^{24} D/m^2, the variations in the measured yield are small, indicating an approach to a constant steady-state value.

For comparison, the data obtained in the PISCES-A experiment [12] is additionally shown in figure 1(a). This data was obtained at a bombarding energy of 140 eV/D^+ (the PISCES-A plasma includes also D_2^+ and D_3^+ as mentioned, but their contribution to the sputtering was assumed negligible due to the lower energy of these ions). The evolution of the sputtering yield with fluence in PISCES-A is qualitatively consistent with the results of our study with a mono-energetic ion beam. Nevertheless, the final yield value of ~ 1.5×10^{-3}, that has resulted at PISCES-A, is lower than that obtained from the 100 eV/D irradiation in this study. A possible explanation is that in PISCES-A a fraction of the sputtered atoms could be ionized in the plasma and redeposited onto the surface. This can lead to an underestimation of the primary (gross) erosion yield. Even though the plasma exposure was performed in the redeposition-suppressed regime (i.e. at rather low fluxes of the order of 10^{21} D/m^2/s) in PISCES-A, redeposition might not have been avoided completely.

3.1.2. A simple analytical approach to describe the yield reduction

An analytical treatment based on a simple dynamic model that considers the balance of atomic species within a thin surface layer is suggested as a first attempt to describe the experimental results. The thickness of this surface layer (called the interaction layer) is taken as constant and can be thought of as being of the order of either the escape depth of sputtered atoms or the ion mixing range. Only this thin layer will be subject to composition changes. EUROFER steel is in reality a multi-elemental (and multi-phase) alloyed material. Within the model, it is treated as a homogeneous amorphous mixture of Fe and W, i.e. other elements as well as phases, crystallinity and grain orientation (and thus grain-dependent sputtering) are ignored. In addition, density changes that would arise as a consequence of composition changes are neglected. The sputtering yield of other major constituents besides Fe and W (mostly mid-Z elements such as Cr) is assumed similar to that of Fe. Therefore, only W is treated separately. Furthermore, the sputtering yields of Fe and W in the interaction layer are assumed identical to those of the pure materials, independent of the composition of the matrix material from which they are sputtered. (This assumption is generally not valid and a more realistic treatment is provided by the SDTrimSP simulations discussed further below.) Within this simple approach the total sputtering yield Y can be written as

$$Y(E,t) \sim Y_{Fe}(E)\frac{N^{Fe}(t)}{(N_0^{Fe}+N_0^{W})} + Y_W(E)\frac{N^{W}(t)}{(N_0^{Fe}+N_0^{W})}.$$

Here, $Y_{Fe}(E)$ and $Y_W(E)$ are the sputtering yields of pure Fe and pure W at the given D bombardment energy E. $N^{Fe}(t)$ and $N^w(t)$ are the atomic areal densities of Fe and W integrated over the interaction layer at time t after the onset of D irradiation. $N_0{}^{Fe}$ and $N_0{}^W$ are the initial integrated atomic areal densities of Fe and W in the interaction layer as deduced from the bulk densities and the assumed thickness of the interaction layer. Therefore, $N^{Fe}(t)/(N_0{}^{Fe}+N_0{}^W)$ and $N^W(t)/(N_0{}^{Fe}+N_0{}^W)$ correspond to the surface concentrations of Fe and W (averaged over the thickness of the interaction layer). Since the atomic fraction of Fe is much higher than that of W and furthermore $Y_{Fe}(E) >> Y_W(E)$ in most of the energy range, the EUROFER erosion is dominated by Fe sputtering (as mentioned above, the contribution of W sputtering was also neglected in the experimental data evaluation). Therefore, the equation can be further simplified to

$$Y(E,t) \sim Y_{Fe}(E)\frac{N^{Fe}(t)}{(N_0^{Fe}+N_0^W)} \quad (1).$$

The time evolution (i.e. the fluence dependence) of the sputtering yield can be deduced once an expression for the time evolution of the Fe areal density in the interaction layer $N^{Fe}(t)$ is provided. This time evolution of $N^{Fe}(t)$ can be described by

$$\frac{dN^{Fe}(t)}{dt} = -Y_{Fe}J_D\frac{N^{Fe}(t)}{(N_0^{Fe}+N_0^W)} + \frac{N_0^{Fe}}{(N_0^{Fe}+N_0^W)}\left(Y_{Fe}J_D\frac{N^{Fe}(t)}{(N_0^{Fe}+N_0^W)} + Y_WJ_D\frac{N^W(t)}{(N_0^{Fe}+N_0^W)}\right) \quad (2),$$

where J_D is the D ion flux. The first term on the right hand side describes the rate at which the Fe areal density in the interaction layer is reduced. The second term corresponds to the flux density of Fe into the interaction layer from underneath due to the material removal by sputtering. (As mentioned, the interaction layer has constant thickness and density changes due to the varying composition in this layer are neglected.) Eq. (2) can be rearranged to separate the variables and then integrated to yield

$$\ln\left(N^{Fe}(t) - \frac{Y_WN_0^{Fe}(N_0^{Fe}+N_0^W)}{Y_{Fe}N_0^W+Y_WN_0^{Fe}}\right) = -\frac{Y_{Fe}N_0^W+Y_WN_0^{Fe}}{(N_0^{Fe}+N_0^W)^2}J_Dt + \ln C\,,$$

with an integration constant C. To get to this result, $N^W(t)$ has been replaced by $(N_0{}^{Fe}+N_0{}^W)$ - $N^{Fe}(t)$. Since the areal density $N^{Fe}(t)$ at $t = 0$ is $N_0{}^{Fe}$, the constant C can be determined to

$$C = N_0^{Fe}\left(1 - \frac{Y_W(N_0^{Fe}+N_0^W)}{Y_{Fe}N_0^W+Y_WN_0^{Fe}}\right).$$

Consequently, the solution to eq. 2 is

$$N^{Fe}(t) = N_0^{Fe}\left(1 - \frac{Y_W(N_0^{Fe}+N_0^W)}{Y_{Fe}N_0^W+Y_WN_0^{Fe}}\right)exp\left(-\frac{Y_{Fe}N_0^W+Y_WN_0^{Fe}}{(N_0^{Fe}+N_0^W)^2}J_Dt\right) + \frac{Y_WN_0^{Fe}(N_0^{Fe}+N_0^W)}{Y_{Fe}N_0^W+Y_WN_0^{Fe}} \quad (3).$$

Since the fluence is defined as $\Phi = J_D{\cdot}t$, the fluence dependence can be deduced from the time evolution by replacing $J_D{\cdot}t$ by Φ. According to eqs. (1) and (3), the fluence dependence of the sputtering yield can be finally expressed as

$$Y(E,\Phi) \sim A(E)exp\left(-\frac{\Phi}{F(E)}\right) + B(E) \quad (4),$$

where

$$A(E) = \frac{Y_{Fe}(E)N_0^{Fe}}{(N_0^{Fe}+N_0^{W})}\left(1-\frac{Y_W(E)(N_0^{Fe}+N_0^{W})}{Y_{Fe}(E)N_0^{W}+Y_W(E)N_0^{Fe}}\right) \quad (5),$$

$$F(E) = \frac{(N_0^{Fe}+N_0^{W})^2}{Y_{Fe}(E)N_0^{W}+Y_W(E)N_0^{Fe}} \quad (6)$$

and

$$B(E) = \frac{Y_{Fe}(E)Y_W(E)N_0^{Fe}}{Y_{Fe}(E)N_0^{W}+Y_W(E)N_0^{Fe}} \quad (7).$$

This states that the yield reduction is expected to decay exponentially (with an offset) as *a priori* assumed in the previous work [12]. $F(E)$ is the characteristic parameter equivalent to the fluence for yield reduction to $1/e$. $B(E)$ is the yield at $\Phi \rightarrow \infty$, corresponding to the final steady-state yield value, and the summation of $A(E)$ and $B(E)$ is the yield at $t = 0$, which is approximately equal to the yield value of pure Fe.

Within this description the energy-dependent parameters *A(E)*, *F(E)* and *B(E)* can be calculated if the sputtering yields of the pure materials Y_{Fe}, Y_W as well as the initial areal densities of Fe and W within the reaction layer are known. It is, as a first step, reasonable to apply known or theoretical values to obtain analytical yield curves from eq. 4. In figure 1, lines labelled as "Analytical (expected)" are the yield reduction curves determined by taking Y_{Fe} and Y_W values from Ref. [10] and assuming an interaction layer thickness of roughly one monolayer, i.e. $N_0^{Fe}+N_0^{W} \sim 2\times10^{19}$ m^{-2}. This assumption is motivated by the very short ion mixing ranges (even below one Å) observed in SDTrimSP simulations. The calculated parameter values according to eqs. (5) - (7) are listed in table 1. With these values, however, the model results do not reproduce the entire experimental data set to a satisfactory extent. For example, the expected analytical sputtering yield curves for D energies of 100 and 200 eV drop faster than the experimental results at higher fluences and they drop steadily within the displayed fluence range with no sign of development towards a steady state. On the other hand, for the higher irradiation energies the analytical curve shows no yield reduction at all, which is also in contradiction to the experimental result for 500 eV/D.

Complementarily, it was attempted to use eq. (4) with $A(E)$, $B(E)$ and $F(E)$ as empirical fit parameters. The resulting fits are labelled 'Analytical (fit)' in figure 1. They show reasonable agreement with the experimental data. The parameter values for $A(E)$, $B(E)$ and $F(E)$ obtained by the fitting are listed in table 1 together with the corresponding calculated ('expected') values. When comparing the theoretically expected and empirically fitted parameter values one can see that a higher value for $F(E)$ than expected is always required to improve the fit to the data. According to eq. (6), $F(E)$ is strongly influenced by the areal atomic density in the interaction layer, $N_0^{Fe}+N_0^{W}$. Recent (yet unpublished) experiments where EUROFER was exposed to a 17 kV hydrogen beam in the GLADIS device [19] have shown W enrichment up to depths far beyond the expected ion mixing range and also far beyond any enriched layer thicknesses predicted by SDTrimSP [20]. In view of those results, a larger value for *F(E)* would be reasonable, due to a thicker interaction layer. As a consequence, the validity of the short ion mixing range and the thin W enrichment layers observed in SDTrimSP would have to be doubted.

For the final steady-state yield $B(E)$, the sputtering yield of W, Y_W, has a key role. The 'expected' Y_W used here was taken as the one of pure W. Consequently, $B(E)$ for 100 and 200 eV/D has to be zero because those energies are below the sputtering threshold for pure W. However, the experimental results require a finite $B(E)$, indicating that Y_W is apparently not zero. In fact, it can be easily shown based on head-on two-body collisions that sputtering below the threshold for pure W is possible via an intermediate collision with Fe. Such multistep collision processes reduce the effective threshold energy for W upon D bombardment to about 100 eV. Another factor contributing to the larger empirical *B(E)* can be an increase in sputtering yields due to a decrease of the surface binding energies (SBE). SBEs are a critical factor for the evaluation of sputtering. For pure materials they are taken equal to the heats of sublimation, i.e. 4.28 eV for Fe and 8.79 eV for W. There are various models for the calculation of SBEs in a mixture of elements. (Several are implemented in SDTrimSP; see also the next section *3.1.3.*) Generally, these models yield a SBE for W in the mixed Fe-W system that is lower than that of pure W. This means that the sputtering of W atoms in a Fe matrix is easier than in a W matrix. The impact of SBEs on the sputtering yield has been considered in the numerical simulations presented in the next section.

It is concluded that, while an exponential function yields a reasonable fit to the experimentally observed sputtering yield evolution, the proposed analytical model appears to be too simple, neglecting important processes.

3.1.3. Comparison to numerical simulations

The decision whether to use steel walls in a future fusion power plant will have to be based on numerical simulations of the erosion taking the energy and species distribution of the impinging particles into account. A widespread code for the simulation of sputtering is SDTrimSP. This is a Monte-Carlo simulation code treating atomic collisions in the binary collision approximation (BCA). It allows dynamic simulations, where the changes in stoichiometry due to implantation and sputtering are taken into account [21, 22]. In the version that is employed here, concentration profiles are one-dimensional, targets being discretized in homogeneous slabs of material. We have previously confirmed that SDTrimSP can well reproduce the experimental sputtering yields for some pure materials that are contained in RAFM steels, namely Fe, Cr and W [10]. In this study, dynamic sputtering simulations were performed with SDTrimSP5.08 [22, 23] (slightly modified for our purpose as detailed further below) for a binary target consisting of Fe and W with a W concentration of 0.33 at.%, thus mimicking the nominal composition of EUROFER. The program requires a number of input parameters, which also include the selection of available models for the simulation of various physical processes. As mentioned in the previous section, one of the important factors for these sputtering simulations is the atomic surface binding energies (SBEs). Generally, in SDTrimSP the SBEs for the pure materials are taken from the heat of sublimation. Several models are implemented for the calculation of SBEs in multi-component

systems. Usually the effective SBE of each target component is calculated as a weighted average taking into account the elemental composition at the surface, e.g. for Fe:

$$SBE_{Fe} = SBE_{Fe-Fe} \cdot c_{Fe} + SBE_{Fe-W} \cdot c_w$$

Here c_{Fe} and c_W are the surface atomic fractions of Fe and W, i.e. the respective concentrations in the first slab of the modelled target. $SBE_{Fe\text{-}Fe}$ is the SBE for pure Fe (4.28 eV). For the SBE of Fe to W, $SBE_{Fe\text{-}W}$, an arithmetic average of the values for the pure materials has been chosen:

$SBE_{Fe-W} = \frac{1}{2}(SBE_{Fe-Fe} + SBE_{W-W})$ (8).The SBE of pure W, $SBE_{W\text{-}W}$, is 8.79 eV. Other important calculation options were set as previously applied to the calculations for pure materials [10], e.g. the Kr-C potential [24] was chosen as the interaction potential and the inelastic stopping power was approximated using an equipartition of Lindhard-Scharff [25] and Oen-Robinson [26] models. For calculation of the scattering integral, the Gauss-Legendre quadrature was chosen instead of the previously used MAGIC method, following the recommendation in [27]. Deuterium accumulation in the sample was not allowed, i.e. the D concentration is kept at zero. This corresponds to the assumption of instantaneous out-diffusion of deuterium whenever the concentrations exceed negligible values.

Furthermore, it was chosen to take into account threshold energies for the movement of recoils by setting the irc0 parameter to 1 [27]: Recoiled atoms that are not sputtered, are replaced to their layer of origin if their starting energy was below 17 eV in the case of Fe and below 38 eV in the case of W. This choice is stressed here, because the default option in SDTrimSP (at least up to the version 5.08) is to neglect displacement thresholds. This neglect would correspond to the situation in the gas phase rather than in an amorphous solid. In many cases the choice of irc0 has no noticable impact on the resulting depth profiles. In the case of shallow surface enrichment and very fine discretization of the target (as described in the next paragraph) this choice is, however, critical.

Typically, in SDTrimSP the targets' depth profile is discretized with slab thicknesses of at least an atomic monolayer, i.e. roughly 2 Å. In the system at hand, this however leads to slab merging artefacts due to the shallow surface enrichment. As has been also observed by von Toussaint et al. [23], these artefacts are avoided by choosing a finer discretization, in our case 0.1 Å. As the physical interpretation of displacements far below interatomic distances, we propose corrugation on an atomic scale, which is certainly present at a surface that has been amorphized by ion bombardment. The problem of artificial enrichment of Fe in the first slab (as well observed in [23]) was resolved by distributing atoms that end up in the first slab over the first 2 Å. This is again justified by the assumed surface corrugation within a thickness of at least one atomic monolayer.

Figure 2 shows the steady state depth profiles that evolve in the SDTrimSP simulation at the various D ion energies. It can be seen that the thickness of the W-enriched surface layer decreases with increasing ion energy. This may appear counter-intuitive at first glance, since it is expected that the average depth of origin of sputtered Fe atoms increases with increasing energy. However, the dominant mechanism governing the enrichment layer thickness is its thinning by W sputtering, which is of course enhanced at the higher energies. Only at 100 eV/D the W concentration reaches 100 at.% in the

simulation. With increasing energy, the difference in sputtering yields between Fe and W decreases and at the same time erosion of the enrichment layer occurs. This leads to decreasing maximum W concentrations. At 1000 eV/D the steady state W depth profile peaks at the surface at a value of roughly 15 at.%. Generally, the resulting W-enriched layers are extremely thin, decreasing from 2.5 Å at 100 eV/D to about 0.1 Å at 500 and 1000 eV/D, which is of the order of the chosen discretization. As mentioned before such small 'layer thicknesses' could be interpreted as atomic corrugation. However, it has to be clearly stated that such steep concentration gradients stretch the physics model of SDTrimSP. Molecular dynamics simulations would be a more appropriate approach for describing the system at these length scales.

The evolution of the sputtering yield that results from the SDTrimSP simulations is shown together with the experimental data in figure 1. The simulation for 100 eV/D (fig. 1 (a)) shows a strong yield reduction with increasing D fluence. At the lowest fluence, the simulated sputtering yield is in agreement with the experimental result. However, the reduction with increasing fluence is faster in the simulation. Above 10^{24} D/m^2 the simulated yield steeply drops: At 4×10^{24} D/m^2 it amounts to 1.6×10^{-4} (out of scale in figure 1(a)), which is more than an order of magnitude smaller than the measured value of 2.1×10^{-3}. Furthermore, the simulated yield continues to drop toward zero, while the experimental values (in particular those from the PISCES-A experiment [12], where higher fluences were achieved) hint at a steady state for fluences beyond 2×10^{24} D/m^2. (An additional data point is outside of the fluence range in figure 1(a), cf. [12]). The second drop in the sputtering yield, that is visible in this double logarithmic plot beyond fluences of several 10^{23} D/m^2, is indicative of two different mechanisms causing continued sputtering yield reduction, each dominating in a distinct fluence regime. The understanding of the physics of these mechanisms is a matter of ongoing investigations.

For 200 eV/D (fig. 1 (b)), the simulation evolves into a steady state in the fluence range beyond 1×10^{23} D/m^2 at a sputtering yield of about 1.5×10^{-2}. On pure W the expected sputtering yield at 200 eV/D would be considerably smaller. As mentioned earlier, W sputtering is increased in the presence of Fe due to sequential collisions between D, Fe and W. However, the simulations are in clear contradiction to the experiment, where the sputtering yield is observed to drop to 3.3×10^{-3} at fluences reaching > 5×10^{24} D/m^2. Note that a second drop (as seen for 100 eV/D) does not appear in the simulations for the higher D energies: The sputtering yield clearly becomes constant – unlike for 100 eV/D, where it always features a negative slope throughout the whole plotted fluence regime. Only very moderate yield reductions are observed in the simulations for 500 and 1000 eV/D (figs. 1 (c) and (d)). For these energies, a steady state develops already at fluences beyond 10^{22} D/m^2. For 1000 eV/D, this is in agreement with the experimental data. The steady state sputtering yield of about 5.3×10^{-2} agrees also reasonably well with the experimental one of 4.4×10^{-2}. For 500 eV/D however, the experiment shows a reduction in the sputtering yield (down to 2.0×10^{-2} at 2×10^{24} D/m^2) that is not reproduced in the simulations (steady state sputtering yield of 4.3×10^{-2}). In the simulations at 500 and 1000 eV/D the sputter yields feature a minimum at an intermediate fluence before increasing towards the steady state value. The reason for

this is the initially higher escape depths for Fe (because of lower stopping power), which somewhat decrease (stopping power increasing) at higher fluence as the W concentration at the surface increases. The magnitude of this effect is far below the sensitivity of the experimental sputter yield measurement. Overall, the SDTrimSP simulations do not satisfactorily reproduce the fluence dependence of the sputtering yields. For the lower energies of 200 and 100 eV/D the simulated steady state sputtering yields deviate by more than an order of magnitude from the experimental ones.

3.2. Surface composition and topography

Figure 3 shows raw RBS spectra obtained from un-irradiated and D-irradiated EUROFER samples in this study. Under the employed measurement conditions (1.0 MeV $^4He^+$ beam with 75° incident angle), the energies of $^4He^+$ species backscattered from Fe and W at the surface are about 750 and 920 keV, respectively. Thus, the spectrum in the energy range from 750 to 920 keV reflects the depth profile of W up to a depth of about 30 nm as indicated by the depth scale in figure 3 (a). At larger depths (backscattering energies below 750 keV), the W spectrum is hidden due to the much larger signal from Fe. A conversion of these spectra into depth profiles is hampered by the influence of surface topography, c.f. figure 6. Nevertheless, it can clearly be seen that the W concentration is enriched at the surface (around 900 keV) after D ion irradiation, and the enrichment becomes more pronounced with increasing D fluence. It should be pointed out that the smearing-out of the Fe edge with increasing fluence is not attributed to changes in the Fe concentration (which are small in relative terms and would not significantly affect the Fe signal intensity), but instead to the evolving surface roughness. The evolution of W enrichment depends also on the D irradiation energy. At 100, 200 and 500 eV/D the W-enriched regions become wider with increasing fluence, extending over several tens of nm at the higher fluences. These depths are far beyond the nominal depth resolution (on a smooth surface) of 3.5 nm. In contrast, at 1000 keV/D the enrichment remains limited to a shallower region. In principle, such an observation could be qualitatively explained considering that at this elevated energy considerable sputtering of W takes place, which will lead to the erosion (and thus thinning) of the enriched surface layer. However, all spectra are likely broadened by the influence of the developing surface topography, which will likely also depend on the ion energy. This precludes a straightforward interpretation. In the cases of irradiation at 500 and 1000 keV, the profiles obtained after fluences of 1.0 and 2.0×10^{24} D/m^2 are almost the same, suggesting that the surface composition reached equilibrium. This is consistent with the constant sputtering yield in this fluence range for both energies.

Figure 4 shows depth profiles of the W concentration determined by the sputter-XPS technique after a series of D irradiations. Only the W concentration (in the Fe matrix) is considered here. The Cr concentration is not included in the evaluation because its depth profile is dominated by interdiffusion and segregation upon exposure to air after the D irradiation and not by the D irradiation itself. This is concluded from the fact, that Cr depth profiles on un-irradiated and irradiated samples are very similar.

The oxygen depth profile is neglected as well in the evaluation and not shown, since oxidation occurs after exposure. We focus here only on the influence that D irradiation has on the W concentration. As indicated by the approximate depth scale given in figure 4 (a), the XPS measurement provides finer profile structure thanks to the better depth resolution compared to the presented RBS measurements. The measurement prior to any Ar sputtering is not shown, because it is strongly influenced by adsorbed impurities (oxygen and carbon) and thus not trustworthy. The first data point shown results from XPS measurements after a sputter fluence of 7.8×10^{14} Ar/cm^2. The W concentration profiles show qualitative agreement with the RBS results: for all energies between 100 and 500 eV the surface peak increases with D fluence. Maximum W concentrations of 5 – 10 at.% are observed at the very surface after 10^{24} D/m^2 of D irradiation. Only for 1000 eV/D the peak concentration is constant (at around 5 at.%) already at 10^{23} D/m^2. As in the case of the RBS spectra, the profiles' features have widths considerably beyond the ion mixing range and it must be pointed out that they could be strongly influenced by the developing surface morphology.

The distribution of W in EUROFER is inhomogeneous as can be seen in figure 5: The top SEM image shows typical lath martensite grain structure [28] and some precipitations as white dots on the un-irradiated EUROFER surface. The size of the precipitates is tens of nanometres, while steel grains exhibit a size of mostly between 1 and 10 micrometres. The bottom image is an energy-dispersive X-ray emission (EDX) intensity map showing the lateral W distribution. It can be seen that part of the total W concentration is present in the form of W-rich precipitates at grain boundaries. The majority of the W is in solid solution in the Fe matrix [29]. Figure 6 shows SEM images of EUROFER at higher magnification prior to D irradiation (a) and after irradiation by 200 eV/D to a fluence of 1.0×10^{24} D/m^2 (b and c). There are also some bright particles along the grain boundaries, which are precipitates containing high-Z elements. These precipitates become more clearly visible after D ion irradiation as seen in figure 6 (b).

Since the precipitates feature high concentrations of W compared to the surrounding grains, they are less easily eroded upon D irradiation. This can entail the accumulation of precipitates at the surface with increasing fluence, which could contribute to the evolution of the measured W profiles. The surface topography that evolves upon erosion varies from grain to grain. In the higher-magnified image (figure 6 (c)), one can clearly see that fine needle-like structures appear on many grains but not on all of them. Such grain-orientation dependence was already observed in Ref. [13]. This surface topography development can be a strong contributing factor to the evolution of the measured W profiles.

Surface topography development affects the erosion behaviour due to the change of exposed surface area, incident angle of projectiles as well as redeposition of sputtered particles. Moderate roughness leads to small variations in the angle of incidence. At low angles (with respect to the surface normal), the expected sputtering yield enhancement with increasing angles is small (see e.g. Ref. [16]). As the roughness (or more precisely the aspect ratios of the surface features) increases, the influence of re-deposition becomes more prominent and in fact tends to dominate according to Ref. [30]. Both the

analytical model and the SDTrimSP simulations presented in the previous section are based on the assumptions that the target is amorphous, with W being homogeneously distributed in the Fe matrix and no effects of surface morphology (changes) induced by the D irradiation are taken into account. As can be seen from the SEM images, this assumption is not fulfilled. The surface topography might critically influence the erosion behaviour. For simulations that are more realistic, it will be necessary to consider also effects of surface topography in the analytical model or 2D-/3D-simulations and to take into account the inhomogeneous W distribution.

4. Summary and outlook

The erosion behaviour of EUROFER steel upon deuterium (D) ion bombardment was investigated under well-defined laboratory conditions. The experimental results show that for D energies between 100 and 500 eV/D the sputtering yield decreased with increasing fluence. At large fluences, a dynamic steady state is expected. A pronounced reduction of the yield with increasing fluence by almost one order of magnitude is observed for impinging D energies of 100 and 200 eV/D. At 500 eV/D, the reduction is limited and at 1000 eV/D, no considerable yield reduction is observed experimentally.

The experimental results are compared to a simple analytic model considering a surface atomic species balance as well as to numerical simulations using the BCA-based Monte-Carlo simulation code SDTrimSP. The proposed analytic model does not correctly describe the experimentally observed sputtering yield evolution. However, the functional dependence (a shifted exponential) that results from this model can reasonably describe the experimental data if the characteristic parameters are determined empirically by using them as fit parameters. The performed SDTrimSP calculations fail to reproduce the experimental results: Considerable discrepancies in the evolution of the erosion yield are observed for irradiation energies of 100, 200 and 500 eV/D. The concentration depth profiles resulting from the simulations feature enrichment layer thicknesses far below one atomic monolayer. It has to be questioned whether the physics model implemented in SDTrimSP can reasonably describe erosion processes where very shallow surface enrichment develops.

Analyses of the surface composition after irradiation reveal increasing W-enrichment at the surface with increasing D fluence. This is qualitatively consistent with the observed sputtering yield reduction. However, the measured depth profiles are probably strongly influenced by the evolution of surface roughness upon D exposure. SEM observations reveal a laterally inhomogeneous (grain-dependent) evolution of surface topography. This fact is neglected in both the analytical model and the SDTrimSP simulations. Considering the surface topography development would likely be the key to improve the quantitative agreement of the models with the experimentally observed reduction of the sputtering yield.

Finally, it should be mentioned that in a reactor environment the first wall is going to be heated during operation. At sufficiently elevated temperatures, the sputtering behaviour is expected to change due to elemental interdiffusion and segregation [31, 32, 13]. The temperature dependence of the steel erosion by well-defined ion bombardment should be investigated in further experiments.

Acknowledgments

Authors acknowledge J. Dorner, M. Fußeder, G. Matern and A. Weghorn for their technical assistances.

This work has been carried out within the framework of the EUROfusion Consortium and has received funding from the Euratom research and training programme 2014-2018 under grant agreement No 633053. The views and opinions expressed herein do not necessarily reflect those of the European Commission. Work was performed under EUROfusion WP PFC

References

[1] B. van der Schaaf, F. Tavassoli and C. Fazio et al., *Fusion Eng. Des,* vol. 69, p. 197, 2003.

[2] K. Ehrlich, *Fusion Eng. Des.*, Vols. 56-57, p. 71, 2001.

[3] R. L. Klueh and A. T. Nelson, *J. Nucl. Mater.,* vol. 371, p. 37, 2007.

[4] N. Baluc, K. Abe and J. L. Boutard et al., *Nucl. Fusion,* vol. 47, p. 696, 2007.

[5] H. Bolt, V. Barabash, W. Krauss, J. Linke, R. Neu, S. Suzuki, N. Yoshida and the ASDEX Upgrade Team, *J. Nucl. Mater.,* Vols. 329-333, p. 66, 2004.

[6] H. Bolt, V. Barabash, G. Federici, J. Linke, A. Loarte, J. Roth and K. Sato, *J. Nucl. Mater.,* Vols. 307-311, p. 43, 2002.

[7] R. Behrisch, G. Federici, A. Kukushkin and D. Reiter, *J. Nucl. Mater.,* vol. 313, p. 388, 2003.

[8] R. A. Pitts, S. Carpentier, F. Escoubriac, T. Hirai, V. Komarov, S. Lisgo, A. S. Kukushkin, A. Loarte, M. Merola, A. Sashala Naik, R. Mitteau, M. Sugihara, B. Bazylev and P. C. Stangeby, *J. Nucl. Mater.,* vol. 438, p. 48, 2013.

[9] R. Lindau et al., *Fusion Eng. Des.,* Vols. 75-79, p. 989, 2005.

[10] K. Sugiyama, K. Schmid and W. Jacob, *Nucl. Mater. and Energy,* vol. 8, p. 1, 2016.

[11] V. K. Alimov, Y. Hatano and K. Sugiyama et al., *Phys. Scr.,* vol. T159, p. 014049, 2014.

[12] J. Roth, K. Sugiyama and V. Alimov et al., *J. Nucl. Mater.,* vol. 454, p. 1, 2014.

[13] M. Balden, S. Elgeti, M. Zibrov, K. Bystrov and T. Morgan, *Nucl. Mater. and Energy,* vol. 12, p. 289, 2017.

[14] A. Manhard, T. Schwarz-Selinger and W. Jacob, *Plasma Sources Sci. Technol.,* vol. 20, p. 015010, 2011.

[15] M. Sode, T. Schwarz-Selinger and W. Jacob, *J. Appl. Phys.,* vol. 113, p. 093304, 2013.

[16] W. Eckstein, C. Garcia-Rosales, J. Roth and W. Ottenberger, "Sputtering Data," IPP Report 9/82 (1993), Max-Planck-Institut für Plasmaphysik, Garching, http://hdl.handle.net/11858/00-001M-0000-0027-6324-6 A(accessed.

[17] M. Mayer, *Nucl. Instr. and Meth. B,* vol. B266, p. 1852, 2008.

[18] R. Behrisch, J. Roth and J. Bohdanski et al., *J. Nucl. Mater.,* Vols. 93-94, p. 645, 1980.

[19] H. Greuner et al., *J. Nucl. Mater.,* vol. 417, p. 495, 2011.

[20] *Private communication by Stefan Elgeti, Thomas Schwarz-Selinger and Udo von Toussaint.*

[21] W. Eckstein, R. Dohmen and A. Mutzke et al., "SDTrimSP: A Monte-Carlo code for calculating collision phenomena in randomized targets," IPP Report 12/3 (2007), Max-Planck-Institut für Plasmaphysik, Garching, http://hdl.handle.net/ 11858/00-001M-0000-0027-04E8-F.

[22] A. Mutzke, R. Schneider, W. Eckstein and R. Dohmen, "SDTrimSP version 5.00," IPP Report 12/08 (2011), Max-Planck-Institut für Plasmaphysik, Garching, http://hdl.handle.net/11858/00-001M-0000-0026-EAF9-A.

[23] U. von Toussant, A. Mutzke, K. Sugiyama and T. Schwarz-Selinger, *Phys. Scr.,* vol. T167, p. 014023, 2016.

[24] W. D. Wilson, L. G. Haggmark and J. P. Biersack, *Phys. Rev. B,* vol. 15, p. 2458, 1977.

[25] J. Lindhard and M. Scharff, *Phys. Rev.,* vol. 124, p. 128, 1961.

[26] O. S. Oen and M. T. Robinson, *Nucl. Instr. and Meth.*, vol. 132, p. 647, 1976.

[27] A. Mutzke, *'SDTrimSP_506_2012.pdf' in the documentation shipped with SDTrimSP: 'News in SDTrimSP Version 5.05'*, 2013.

[28] H. Kitahara, R. Ueji, N. Tsuji and Y. Minamino, *Acta Materialia*, vol. 54, p. 1279, 2006.

[29] V. Oliveira, K. Zilnyk and H. Sandim, *Phase Equilib. Diffus.*, vol. 38, p. 208, 2017.

[30] U. von Toussaint, A. Mutzke and A. Manhard, *Phys. Scr.*, vol. T170, p. 014056, 2017.

[31] V. Alimov, Y. Hatano and N. Yoshida et al., *Nucl. Mater. and Energy*, vol. 7, p. 25, 2016.

[32] R. Koslowski, S. Bhattacharyya and P. Hansen et al., "https://arxiv.org/abs/1803.01800," (Submitted to Condensed Matter), 2018. [Online].

Table 1
Characteristic parameter values for the eq. (4). The "Expected" values are theoretically expected values determined according to eqs. (5) - (6), whereas "Empirical fit" values are derived from the empirical fitting to the experimental results.

	Prefactor A(*E*)		*Decay constant F*(*E*) [D/m^2]		*Offset B*(*E*) [Fe/D]	
	Expected	Empirical fit	Expected	Empirical fit	Expected	Empirical fit
100 eV/D	8.61E-3	6.65E-3	6.94E23	8.22E23	0	1.98E-3
200 eV/D	2.36E-2	2.03E-2	2.53E23	8.60E23	0	3.34E-3
500 eV/D	1.54E-3	2.19E-2	5.74E21	4.28E23	4.02E-2	2.00E-2
1000 eV/D	6.01E-4	5.35E-3	1.90E21	7.83E22	4.83E-2	4.37E-2

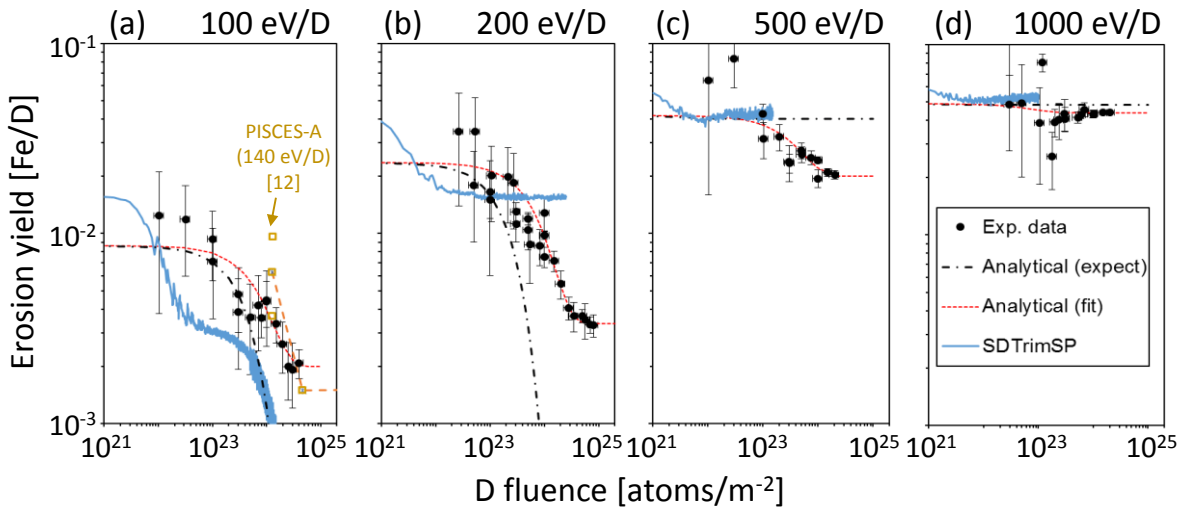

Figure 1

Fluence dependence of the sputtering yield of EUROFER (experimental) and Fe-W (model results and simulations) by irradiation with D at energies of (a) 100 eV/D, (b) 200 eV/D, (c) 500 eV/D and (d) 1000 eV/D. Results obtained in the PISCES-A experiment [12] are included in (a) (symbol: □) for comparison.

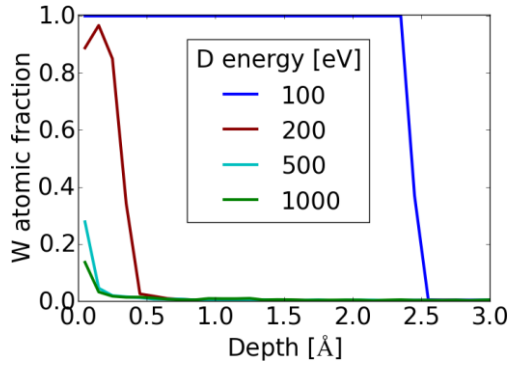

Figure 2

Depth profiles of the tungsten concentration (for various energies of the impinging D ions) in the dynamic steady state that evolves in the SDTrimSP simulations at high fluences.

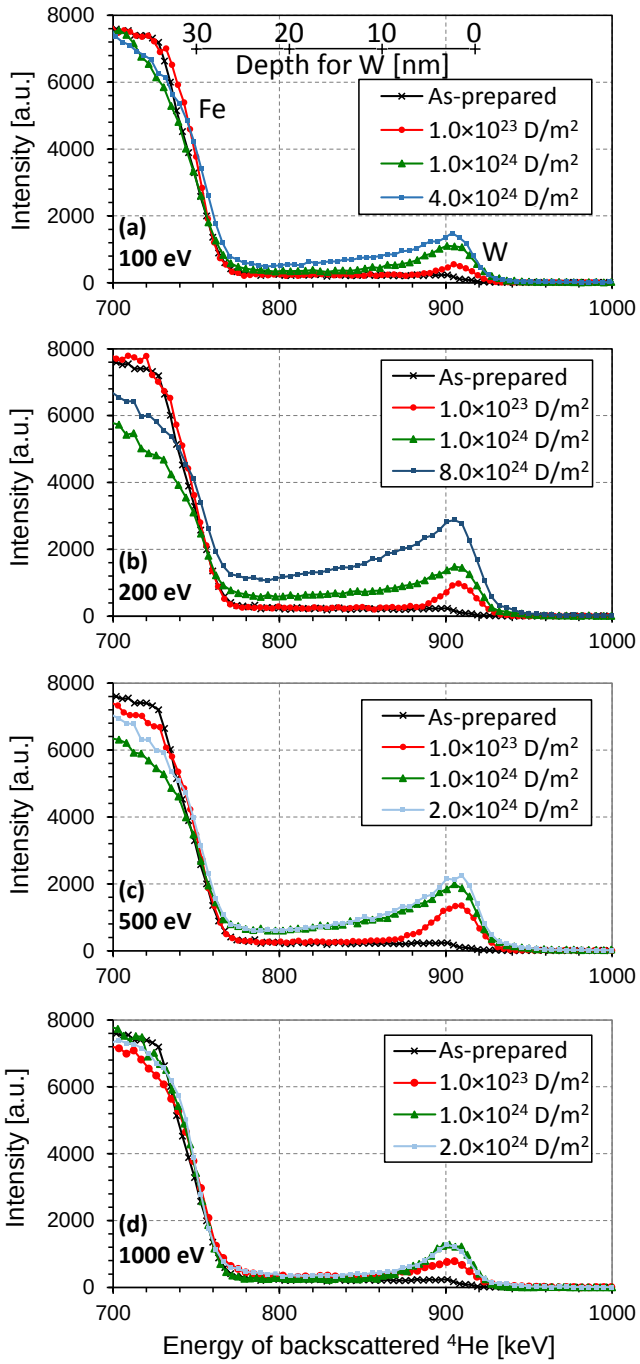

Figure 3

RBS spectra obtained from EUROFER samples after D irradiation with energies of (a) 100 eV/D, (b) 200 eV/D, (c) 500 eV/D and (d) 1000 eV/D to various fluences. Note that the maximum applied fluence varies for the various energies. The spectrum obtained from an un-irradiated sample is also displayed as a reference. Under the employed measurement conditions, the energies of ^{4}He atoms backscattered from Fe and W at the surface are about 750 and 920 keV, respectively. The spectrum shape from 750 to 920 keV corresponds to the W depth profile up to ~ 30 nm. The depth scale for W is given in (a) (valid also for all other cases) as a guide.

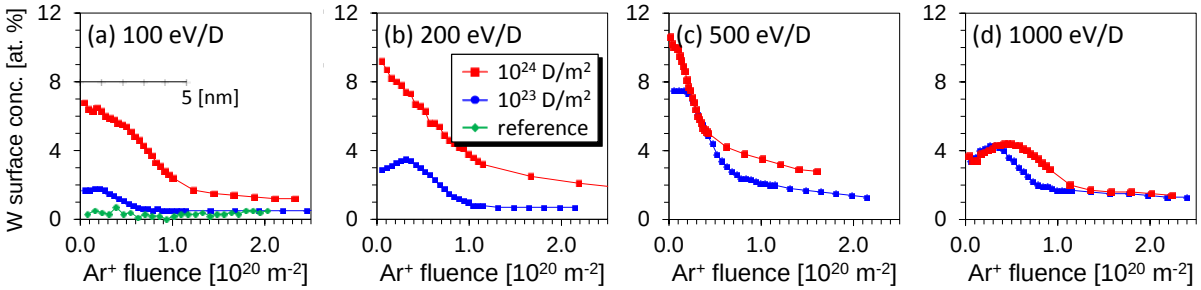

Figure 4

W depth profiles as determined by sputter-XPS before and after D irradiation to two different fluences (1.0×10^{23} and 1.0×10^{24} D/m^2) at various energies: (a) 100 eV/D, (b) 200 eV/D, (c) 500 eV/D and (d) 1000 eV/D. The W concentration is normalized to the sum of the signals from the main metallic constituents, i.e. Fe, Cr and W. In figure (a) the depth profile from prior to D irradiation is shown in addition. The x-axis indicates the Ar^+ fluence applied for the surface sputtering. In an SDTrimSP simulation, the sputtering rate of Fe by 10 keV Ar^+ at 20° incident angle is calculated to be 3.7 Fe/Ar. This value is used to convert the Ar^+ fluence to a depth scale in units of length. The resulting scale bar is shown in (a) and valid for all other cases too. It is only an approximate scale and serves as a guide for the actual depths.

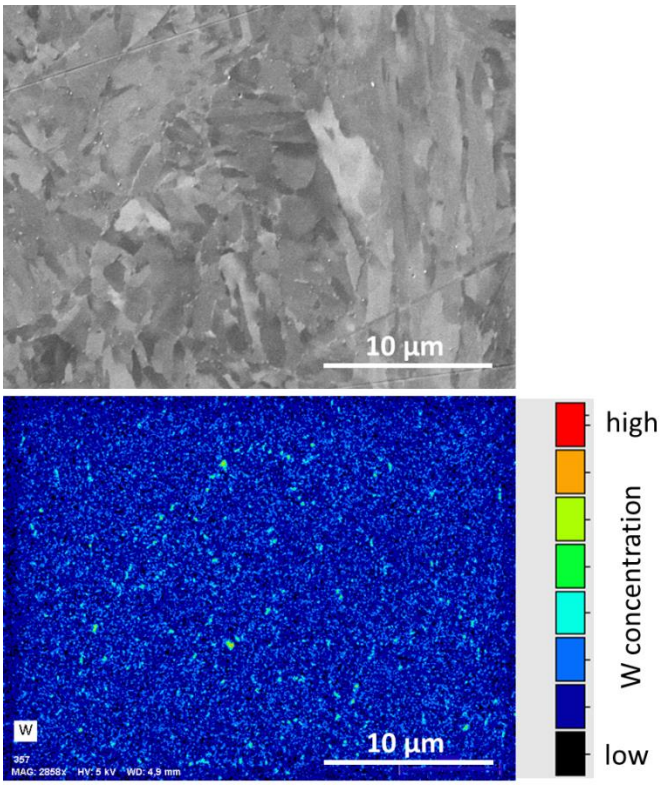

Figure 5

Top: SEM picture of secondary electrons showing the grain structure of EUROFER with W-rich precipitates (bright dots) at grain boundaries. Bottom: EDX-map of the same region showing the distribution of W. The electron energy for both images was 5 keV. The intensities in the bottom image correspond to the background-subtracted and integrated signal from W X-ray emission (M-line).

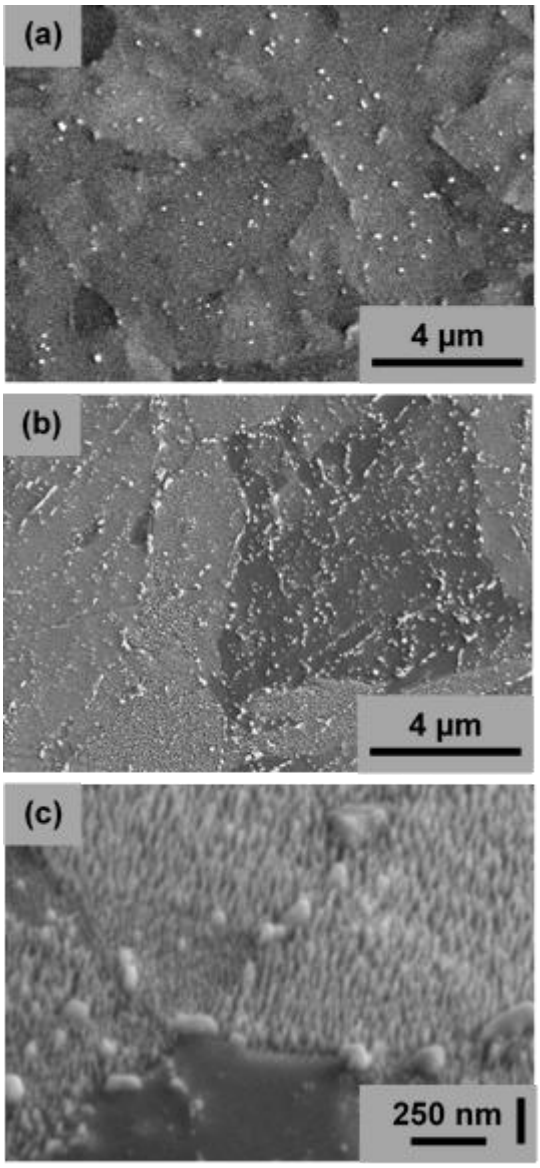

Figure 6

Secondary electron (SE) images obtained from EUROFER samples: (a) prior to D exposure and (b), (c) after 200 eV/D irradiation to a fluence of 1.0×10^{24} D/m^2. Image (c) has higher magnification and the sample was tilted at 52° to better visualize the morphology. Because of the tilt in figure (c), the horizontal and vertical length scales are quantified by different scale bars.